Proceedings of IMECE'02:
2002 ASME International Mechanical Engineering Congress & Exposition
New Orleans, Louisiana, November 17-22, 2002

IMECE2002-33837

RUN-TIME THREE-DIMENSIONAL BLEND-PATH GENERATION FOR COBOT CONSTRAINT SURFACES

Eric L. Faulring
Laboratory for Intelligent Mechanical Systems (LIMS)
Mechanical Engineering - Northwestern University
Evanston, Illinois 60208 USA
e-faulring@northwestern.edu

J. Edward Colgate
Laboratory for Intelligent Mechanical Systems (LIMS)
Mechanical Engineering - Northwestern University
Evanston, Il 60208 USA
colgate@northwestern.edu

ABSTRACT

During human-cobot interaction, transitions often occur between free mode operation and constraint surface following. This paper considers the following typical scenario: an operator of a three-dimensional (e.g. *x-y-z* or *x-y-θ*) cobot commands a "join" from free mode to a one-dimensional constraint path. To ensure that this transition is smooth and responsive, a "blend path" is computed that joins the cobot's initial location to a location on the constraint path. The blend path must match tangency and curvature at each end, and must also exhibit continuous curvature. A novel "triple-clothoid" algorithm is developed that meets these requirements. In addition, we demonstrate that the triple-clothoid is particularly amenable to *x-y-θ* systems via implementation on a planar cobot.

Keywords: cobot, clothoid, curvature, three-dimensional, path generation.

INTRODUCTION

This research endeavors to create a smooth transition between two non-coincident trajectories in three-space. The blend path must match tangency and curvature at each end, must exhibit continuous curvature and must be well behaved with respect to the choice of control points. This path generation research is motivated by experimentation with a planar *x-y-θ* cobot used as a warehousing pallet jack. The three-wheeled "Scooter Cobot," introduced by Peshkin et al. [1], is converted into a "Pallet Jack Cobot" (Fig. 1). A freely pivoting handle, equipped with an encoder, is mounted at the perimeter of the device, and replaces Scooter's force sensor as the input device. Cobots (collaborative robots) are robotic devices by virtue of their computer control and intelligence, but are designed for collaboration with human operators in a shared workspace. The dominant feature of cobots is their ability to safely provide hard and smooth virtual constraint surfaces through the use of non-holonomic steerable joints. In the case of the Pallet Jack Cobot, computer steered wheels that are un-powered about their rolling axes provide these constraints.

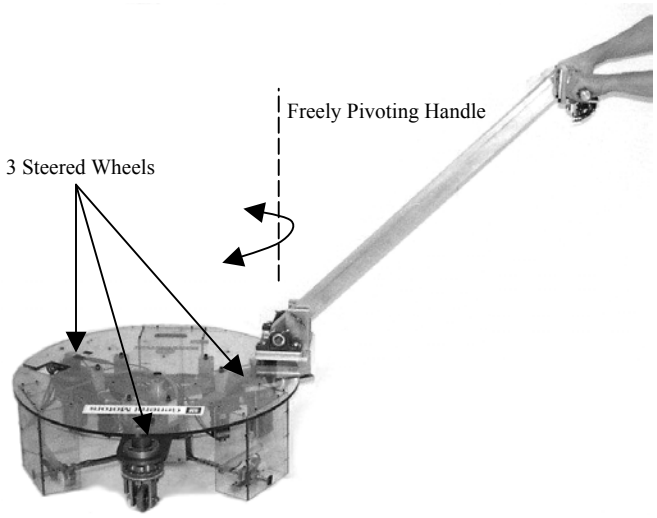

Figure 1. A handle that is fixed vertically and pivots freely in the horizontal plane is added to the three-wheeled "Scooter Cobot" to create a "Pallet Jack Cobot." The wheels are steered by computer control in response to the handle angle or presence of a constraint surface but remain un-powered about their rolling axes.

Tasks involving the merging from a free mode, where the user both steers and pushes/pulls the cobot, to a constrained one-dimensional path, where the user pushes/pulls but does not steer, are examined here. We consider merging to a trajectory down the center of a warehouse aisle or executing a dock with a recently acquired target.

There are numerous types of curves applicable to the generation of paths in three dimensions. However, most solutions ignore tangency and curvature requirements at the start and end of the path and few consider the ergonomic cost of a path. Bézier curves and cubic B-splines are common solutions to three-dimensional path creation. However, while they can be modified to satisfy tangent and curvature requirements, in addition to start and endpoint positions in three-dimensional space, curvature and higher derivatives along the paths are not easily controlled. In addition, the choice of control points to define spline curves is arbitrary and non-trivial.

Since the desire of this research is to merge two trajectories, and not a large series of control points, one is not limited to such curve definitions as splines. Clothoid curves, capable of merging two trajectories, are an attractive alternative; since clothoids require only two control points and tangents at those points, they are easy to define and there is no ambiguity to the choice of control points. In addition, clothoid curves are appropriate since, by definition, their curvature is defined as a linear function of path length. Curvature starts out at zero for the initial straight-line trajectory, and increases linearly as a function of path length to a maximum value at the midpoint of the clothoid before decreasing linearly. Defining a clothoid in this fashion provides continuous curvature. Thus our desire to maintain continuous acceleration or curvature is built into the clothoid curve's definition. Clothoids are used in highway and railway design as well as roller coaster and ship hull designs.

PLANAR-CLOTHOIDS

Figure 2 depicts a planar-clothoid (used for trajectories which intersect in two or three dimensions) and some associated terminology. The planar-clothoid is defined by points $\boldsymbol{R_1}$ and $\boldsymbol{R_3}$ with initial tangent $\boldsymbol{T_1}$ at start point $\boldsymbol{R_1}$ and final tangent $\boldsymbol{T_2}$ at end point $\boldsymbol{R_3}$. $\boldsymbol{R_2}$ is determined by the intersection of the lines defined by $\boldsymbol{R_1}$, $\boldsymbol{T_1}$, $\boldsymbol{R_3}$ and $\boldsymbol{T_2}$, thus it is coplanar with points $\boldsymbol{R_1}$ and $\boldsymbol{R_3}$. Notation and formulas for planar-clothoids are interpreted from Schmitt and Book [2].

Two cases exist for the use of planar-clothoids: either the application has a specified maximum curvature, ρ (making d a function of ρ), or the application specifies the distance d (making ρ a function of d). The clothoid is defined parametrically as a function of path length s. Formulas to evaluate the planar-clothoid's position vector $\boldsymbol{R(s)}$, unit tangent vector $\boldsymbol{T(s)}$, unit normal vector $\boldsymbol{N(s)}$ and curvature magnitude $\kappa(s)$ are given in the Appendix. Three sets of equations are required; one for the proximal clothoid segment ($0 \leq s < a$), one for distal clothoid segment ($a \leq s < 2a$) and one for the final tangent $\boldsymbol{T_2}$ ($2a \leq s$). Local coordinate frames are created at $\boldsymbol{R_1}$ and $\boldsymbol{R_3}$ for the proximal and distal segments respectively. The basis vectors of these local frames with respect to the global frame are defined in the appendix.

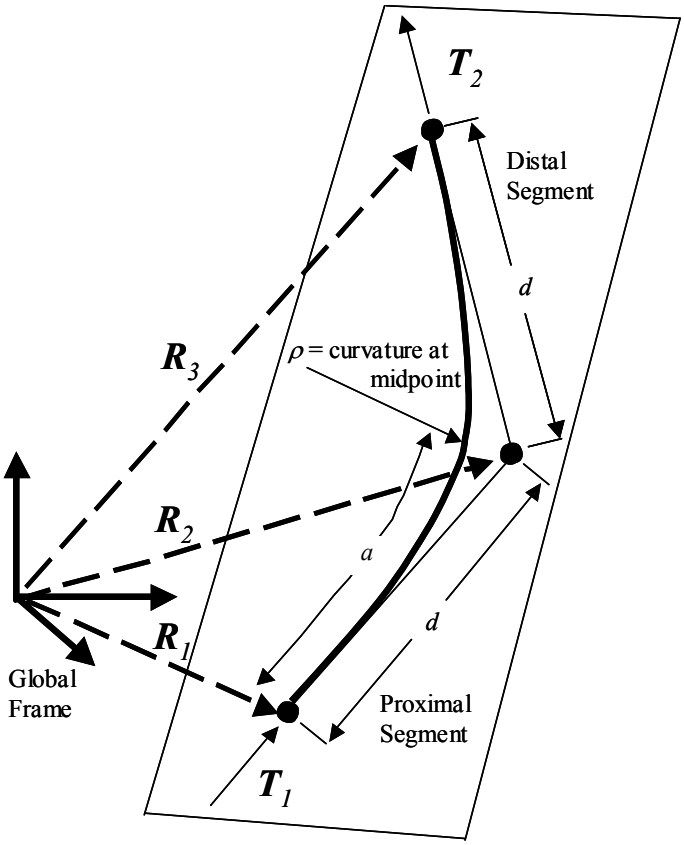

Figure 2. The planar-clothoid geometry consists of two control points R_1 and R_3, at which start and goal tangents T_1 and T_2 are defined.

DERIVATION OF TRIPLE-CLOTHOID

Given two non-intersecting trajectories and the start and goal points on them, a solution curve must smoothly branch off of one trajectory at the start point and join with the other trajectory at the goal point as shown in Fig. 3. The remainder of this paper will abide by the assumption that the initial and final trajectory have zero curvature, or are linear trajectories in a three-dimensional space, thus a solution for matching arbitrary initial and final curvature is not provided.

The construction defined in Fig. 4 better characterizes the space in which the triple-clothoid solution takes place. First, the shortest distance between the two skew lines is found. The shortest distance is perpendicular to both the start and finish trajectories and is a normal to the mid-plane shown in Fig. 3. Figure 4 further defines the desired curve by adding back-planes normal to the mid-plane and projections of the triple-clothoid curve to the mid-plane.

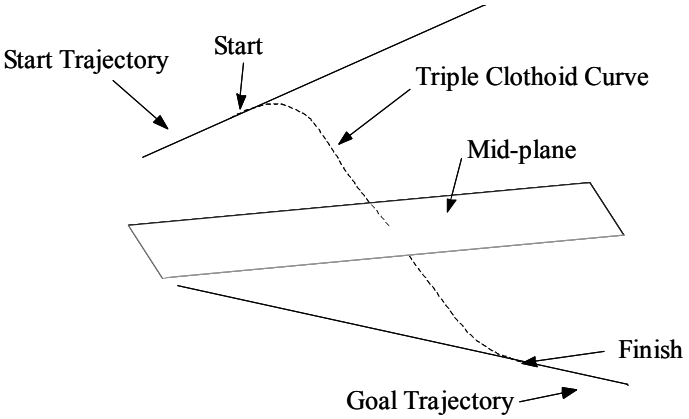

Figure 3. A triple-clothoid trajectory branches off of the start trajectory and merges with the goal trajectory at the start and finish points respectively. A mid-plane is defined by a normal that is the shortest distance between the two non-intersecting trajectories.

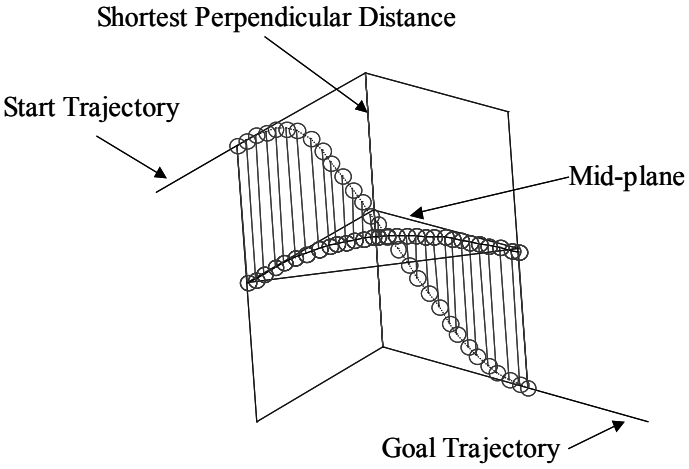

Figure 4. Two planes that are normal to the mid-plane and parallel to the start trajectory and goal trajectory respectively, are added to the construction. Lines of projection from the triple-clothoid curve to the mid-plane are also shown.

The triple-clothoid curve and the lines of projection are laid flat without any distortion of surface area as shown in Fig. 5. The triple-clothoid curve is composed of three planar-clothoids that are now defined. *Clothoid 0* resides in the mid-plane of the construction, and *Clothoids 1* and *2* lie in the two-dimensional flattened projection. *Clothoids 1* and *2* create curvature normal to the mid-plane (torsion of the triple-clothoid curve). *Clothoid 1* turns the start trajectory down towards the mid-plane, and once the triple-clothoid curve passes the mid-plane, *Clothoid 2* turns the curve back toward the goal trajectory.

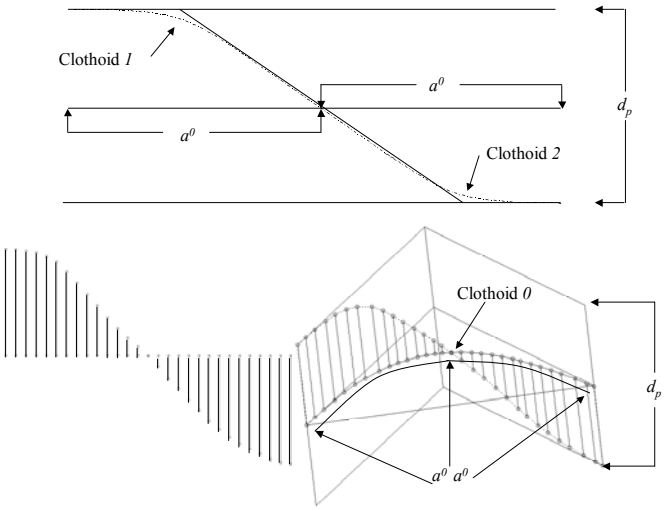

Figure 5. The surface defined by the lines of projection (lower right) is laid flat (lower left) in a plane without distortion of surface area. Arc-length a^0 and shortest perpendicular distance d_p are preserved (upper). *Clothoid 0* is delineated in the mid-plane (lower right) and *Clothoids 1* and *2* in the flattened surface (upper).

The parametric triple-clothoid curve is defined with respect to the parameter *s*, which is the actual path length (see Fig. 6). Since there is no distortion in laying the projection flat, the arc length *s* in the three-dimensional construction and in the flattened projection for *Clothoids 1* and *2* remains the true distance traveled.

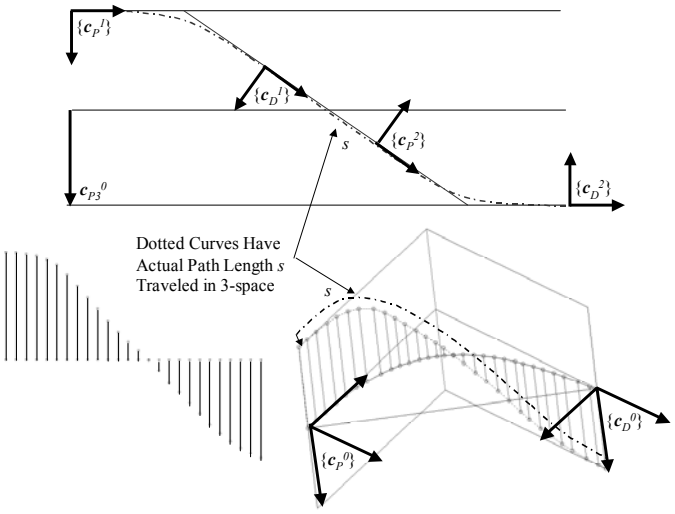

Figure 6. Local coordinate frames for the proximal and distal portions of each clothoid are represented by $\{c_P{}^0\}$, $\{c_D{}^0\}$, $\{c_P{}^1\}$, $\{c_D{}^1\}$, $\{c_P{}^2\}$ and $\{c_D{}^2\}$ frames as defined in the Appendix. The $c_{P3}{}^0$ unit vector is

preserved in the two-dimensional space (upper) after transformation from the three-dimensional space (lower right). Path length *s* is also preserved under this transformation.

Also note in Fig. 6 that the *Clothoid 0 P3* proximal unit vector, $\boldsymbol{c}_{P3}^{\,0}$, is also a unit vector of the flattened two-dimensional projection. Superscripts 0, 1 or 2 in all subsequent notations will indicate to which of the three planar-clothoids a parameter refers. Lack of a superscript indicates a parameter that is general to the whole triple-clothoid construction.

Figure 7 demonstrates the transformation from triple-clothoid path length s to *Clothoid 0* proximal frame coordinates, which are then easily converted to global frame position coordinates $\boldsymbol{R}(s)$. This transformation is also described by Eq. 1.

$$\boldsymbol{R}(s) = \boldsymbol{R}_2^{\,0} + a_{P1}^{\,0}(s)\boldsymbol{c}_{P1}^{\,0} + a_{P2}^{\,0}(s)\boldsymbol{c}_{P2}^{\,0} + a_{P3}^{\,0}(s)\boldsymbol{c}_{P3}^{\,0} \qquad (1)$$

$\boldsymbol{c}_{P1}^{\,0}$, $\boldsymbol{c}_{P2}^{\,0}$ and $\boldsymbol{c}_{P3}^{\,0}$ are the *Clothoid 0* proximal frame basis vectors and $a_{P1}^{\,0}$, $a_{P2}^{\,0}$ and $a_{P3}^{\,0}$ are scalar coefficients. $\boldsymbol{R}_2^{\,0}$ is the intersection point of *Clothoid 0's* start and goal tangents, or the midpoint of the shortest distance between the original skew start and goal trajectories. Similarly, the global frame coordinates for the distal portion of *Clothoid 0* are found via Eq. 2.

$$\boldsymbol{R}(s) = \boldsymbol{R}_2^{\,0} + a_{D1}^{\,0}(s)\boldsymbol{c}_{D1}^{\,0} + a_{D2}^{\,0}(s)\boldsymbol{c}_{D2}^{\,0} + a_{D3}^{\,0}(s)\boldsymbol{c}_{D3}^{\,0} \qquad (2)$$

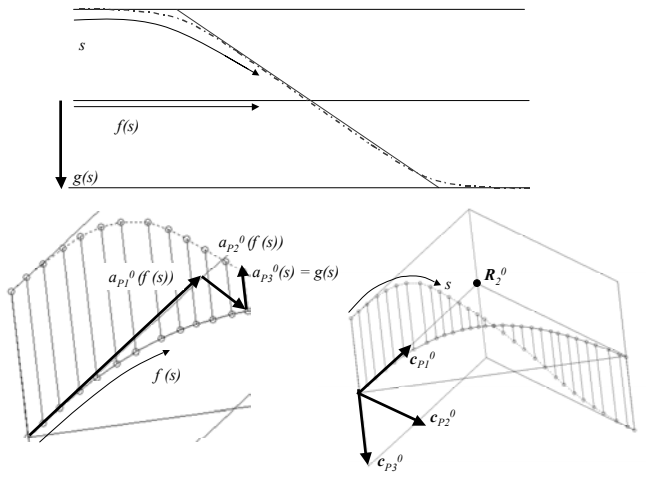

Figure 7. The local frames of *Clothoids 1* and *2* map actual path-length *s* to *f(s)* and *g(s)* which are orthogonal to *Clothoid 0* local frames. *Clothoid 0* local frame coordinates can then be transferred to the global frame. Thus *Clothoid 0* proximal frame coordinates are the following functions of *s*; $a_{P1}^{\,0}(f(s))$, $a_{P2}^{\,0}(f(s))$ and $a_{P3}^{\,0}(s)=g(s)$.

Equations 3 through 5 are used to find the coordinates $a_{P1}^{\,0}$, $a_{P2}^{\,0}$ and $a_{P3}^{\,0}$ (also the coordinates $a_{D1}^{\,0}$, $a_{D2}^{\,0}$ and $a_{D3}^{\,0}$ for the distal portion of *Clothoid 0*). *f(s)* is a distance in the flattened projection, and is a function of the true distance traveled s. $a_{P3}^{\,0} = g(s)$ is a distance in both the three-dimensional space and the flattened projection, and is a function of the true distance traveled s. $a_{P1}^{\,0}$ and $a_{P2}^{\,0}$ are functions of *f(s)*, or functions of a function of s. *f(s)* and *g(s)* are computed from position vector equations evaluated for planar *Clothoids 1* and *2* parametric in s. $a_{P1}^{\,0}(f(s))$ and $a_{P2}^{\,0}(f(s))$ are computed from position vector equations evaluated for planar *Clothoid 0* parametric in *f(s)*.

$$a_{P1}^{\,0} = a_{P1}^{\,0}(f(s)) \qquad (3)$$

$$a_{P2}^{\,0} = a_{P2}^{\,0}(f(s)) \qquad (4)$$

$$a_{P3}^{\,0} = a_{P3}^{\,0}(s) = g(s) \qquad (5)$$

One step thus far ignored in the definition of *Clothoids 1* and *2* of Fig. 5 is the angle the clothoids ramp up to and then down from. The angle is arbitrary, as illustrated by Figs. 8 and 9. a^0 and d_p are fixed parameters but the ratio of l_1 to a^0 is left up to the user's discretion and creates an additional parameter l_3 in Fig. 8 or l_4 in Fig. 9 that defines the triple-clothoid.

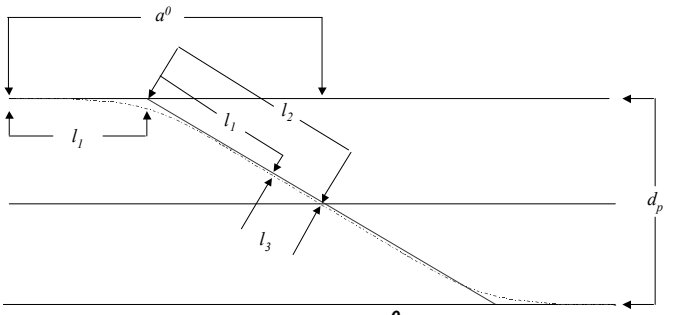

Figure 8. The first case for l_1/a^0 is chosen such that $l_1 < l_2$, $l_3 = l_2 - l_1$, and $l_4 = 0$.

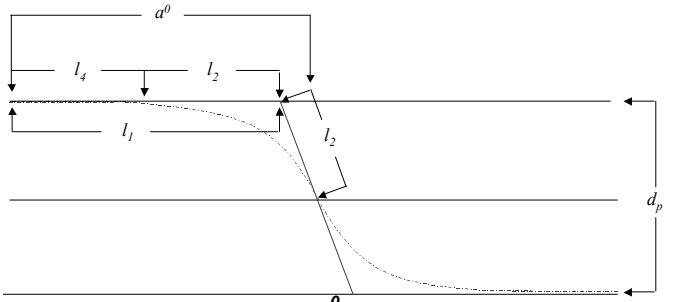

Figure 9. Alternatively l_1/a^0 can be chosen such that $l_1 > l_2$, $l_3 = 0$, and $l_4 = l_1 - l_2$.

The ratio l_1/a^0 impacts the curvature of the triple-clothoid curve. Total space curvature or composite curvature, the Euclidean norm of curvature and torsion, is composed of mid-plane *Clothoid 0* instantaneous curvature and the out-of-plane *Clothoids 1* and *2* instantaneous torsion (see Barnhill [4] and Faux [5] for explanations of space curvature). The mid-plane and out-of-plane curvature and torsion vectors are normal to one another and are orthogonal to the triple-clothoid tangent. The mid-plane curvature, out-of-plane torsion and composite curvature are plotted in Fig. 10 for the curve shown in Figs. 3 through 7 which has $l_1/a^0 = 0.25$. The selection of the ratio l_1 to a^0 affects the shape of the curves in this graph. The case of Fig. 8 spreads the change in the $a_{P3}{}^0$ coefficient out over the length of *Clothoid 0*. The case of Fig. 9 localizes change in the $a_{P3}{}^0$ coefficient to the center region of *Clothoid 0* but will cause steeper slopes in the graph of out-of-plane torsion. Note that *Clothoids 1* and *2* appear as linear changes in out-of-plane torsion with respect to path length of the triple-clothoid. The mid-plane curvature of *Clothoid 0* does not appear to change linearly with path length since it is a linear function of the *f(s)* coordinate derived from *Clothoids 1* and *2*.

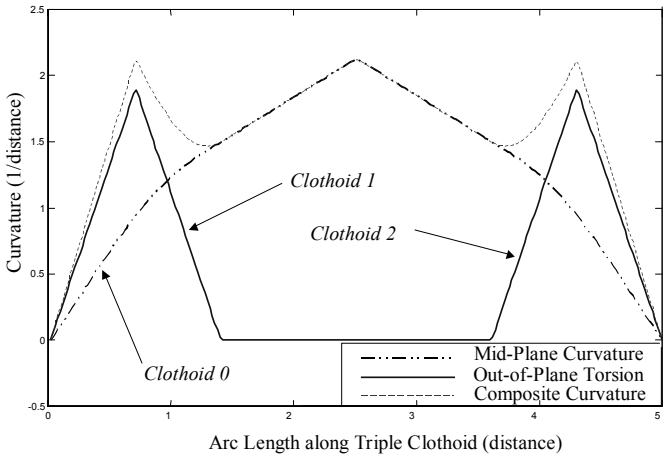

Figure 10. Mid-plane curvature, out-of-plane torsion and composite curvature are plotted versus path length of the triple-clothoid.

IMPLEMENTATION

When the equations to evaluate the coefficients of Eqs. 3 through 5 are compiled, nine separate sets of equations in terms of path length s are found (due to switching between overlapping segments of the parallel definitions of *Clothoid 0* with *Clothoids 1* and *2*). Figure 11 shows these nine segments. In *Segment 1* the proximal portion of *Clothoid 0* is active while the tangent prior to the proximal portion of *Clothoid 1* is active. In *Segment 2* the proximal portion of *Clothoid 0* is active while the proximal portion of *Clothoid 1* is active. In *Segment 3* the proximal portion of *Clothoid 0* is active while the distal portion of *Clothoid 1* is active, etc. Thus different combinations of the portions of position, tangent, and normal equations of planar-clothoids (Eqs. 9 through 12), applied to *Clothoids 0, 1* and *2* result in different formulas for each segment.

The segments each apply to a specific range of triple-clothoid path length s as follows:

$$
\begin{aligned}
&\textit{Segment } 1, \quad 0 \le s < l_4 \\
&\textit{Segment } 2, \quad l_4 \le s < l_4 + a^1 \\
&\textit{Segment } 3, \quad l_4 + a^1 \le s < l_4 + 2a^1 \\
&\textit{Segment } 4, \quad l_4 + 2a^1 \le s < l_4 + 2a^1 + l_3 \\
&\textit{Segment } 5, \quad l_4 + 2a^1 + l_3 \le s < l_4 + 2a^1 + 2l_3 \\
&\textit{Segment } 6, \quad l_4 + 2a^1 + 2l_3 \le s < l_4 + 2a^1 + a^2 + 2l_3 \\
&\textit{Segment } 7, \quad l_4 + 2a^1 + a^2 + 2l_3 \le s < l_4 + 2a^1 + 2a^2 + 2l_3 \\
&\textit{Segment } 8, \quad l_4 + 2a^1 + 2a^2 + 2l_3 \le s < 2l_4 + 2a^1 + 2a^2 + 2l_3
\end{aligned}
\tag{6}
$$

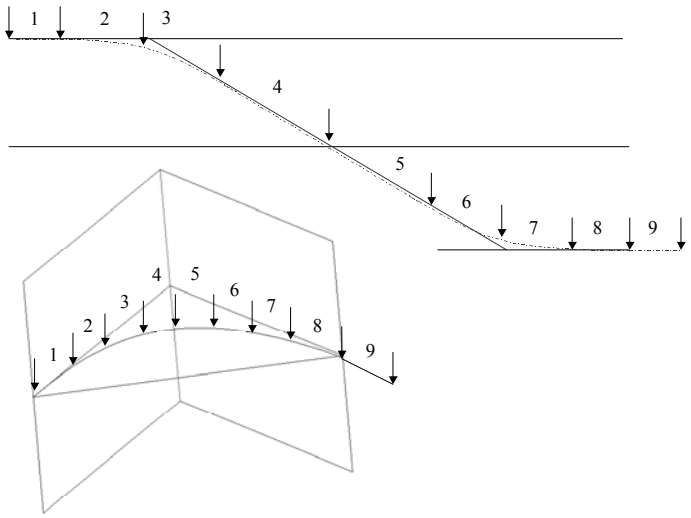

Figure 11. The nine possible segments of a triple-clothoid curve. Note that either segments *1* and *8* will have zero length (case represented in Fig. 8) or segments *4* and *5* will have zero length (case represented in Fig. 9). Figure 11 as drawn does not represent either case since all nine segments have finite length for the purpose of illustration.

The starting global frame tangent defines the path for $s < 0$ and the goal global frame tangent defines the path for $s \ge 2l_4 + 4a^1 + 2l_3$ (*Segment 9*).

Applying Eqs. 3 through 5 in conjunction with Eq. 9 gives the position vector that defines the triple-clothoid path between start and goal trajectories. Unit tangent vectors and unit normal vectors must also be computed for feed forward and feedback control of path following. However, applying the formulas for tangent and normal of clothoids, Eqs. 10 and 11 in the Appendix to the dual functionals of Eqs. 3 through 5 for triple-clothoids, yields rather complicated expressions. Numerical

differentiation of the position vector to obtain tangent direction and normal direction makes the computations more tractable. Equation 12 for curvature magnitudes is, in contrast, easily applied analytically.

As implemented, the triple-clothoid path was broken into 250 segments regardless of length, for which position vectors and curvature magnitude were determined by analytical evaluation. Tangent and curvature vectors were determined by numerical differentiation of the position values. This computation must be efficiently coded so as not to exceed one sampling interval of the control system. Alternatively, the computation of the 250 points could be done over several sampling intervals as needed once the initial construction geometry has been computed. The 250-segment triple-clothoid was found adequate to produce a smooth path even in regions of high curvature.

APPLICATION

The triple-clothoid solution was tested on the afore-mentioned x-y-θ Pallet Jack Cobot and applied to merging to a trajectory down the center of a warehouse aisle. θ is scaled from radians to length so that the definition of the triple-clothoid in an R^3 space still applies. Suppose that an operator is pushing a pallet jack towards an aisle where local sensors pick up a magnetic strip in the floor or global sensors detect a virtual path nearing. A light or sound indicator makes the operator aware that a target trajectory is in sight. The operator can then push a button to accept the new constrained trajectory from the manual mode trajectory that he or she is currently controlling. Subsequent to the operator accepting the target trajectory, the computer calculates a triple-clothoid path to the target trajectory, and then tracks that path to the target. The operator could release himself or herself from path tracking by another push of a button. Recall that we have made the assumption that the initial and goal trajectories be linear paths in three-dimensional space.

The concept of merging to a target trajectory could also be applied to accepting a docking target. A pallet jack might detect an empty parking bay along the side of an aisle. The computer could then compute an exact trajectory aligning position and orientation and, finally, braking by misaligning the cobot's wheels (causing them to disagree on an instantaneous center of rotation) when the target is reached.

Figure 12 displays data for a typical triple-clothoid trajectory merging solution. The x-y projection shows the initial trajectory (left to right) that the operator was on when he or she accepted the detected desired trajectory. The computer then computed the curve that lead to the goal trajectory (upward to the right). In the x-θ projection, it is evident that the initial trajectory had a small θ component while the final goal trajectory does not.

Figure 13 shows data for the same triple-clothoid path found in Fig. 12. The positions of the Pallet Jack Cobot's center of mass and the handle grip with which the operator interacts are displayed. The handle grip path at first deviates to the outside of the triple-clothoid that the cobot follows, as the user attempts to stay behind the Pallet Jack Cobot. Once the cobot reaches the goal trajectory and straightens its path, the handle grip trace moves to a more efficient trajectory inside the triple-clothoid curve. Use of a triple-clothoid path and computer controlled steering eliminates handle steering motions by the operator, and simply requires that the operator maintain the handle sufficiently tangent to the Pallet Jack Cobot's trajectory, so that the pushing or pulling effort is minimized.

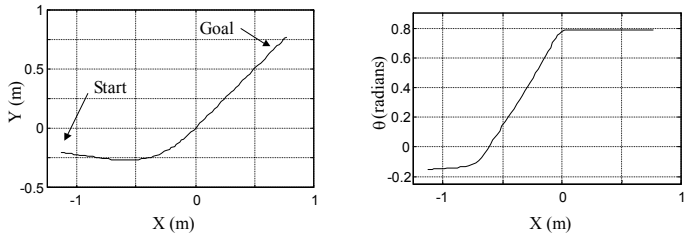

Figure 12. Two projections of a three-dimensional triple-clothoid trajectory for the *x*-*y*-θ Pallet Jack Cobot.

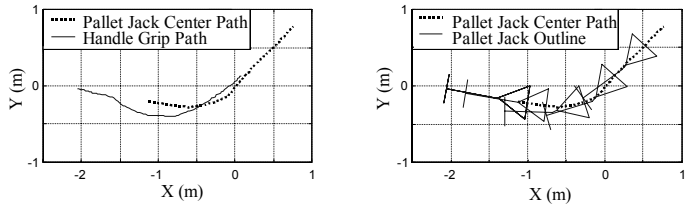

Figure 13. Pallet Jack Path and Handle Path. The solid line of the left plot shows the trace of the handle grip. In the right plot of Fig. 13, an outline of the Pallet Jack Cobot and its handle is shown at half-second intervals.

Chaining multiple triple-clothoids together is another useful exercise. Consider moving down an aisle and needing to dodge around an obstacle. A dodge path like the y-x projection of Fig. 14 might be useful. Three triple-clothoids were combined to do this. The first causes the path to bend slightly upwards. The second causes the path to bend slightly downwards and the third causes the path to level out onto the original trajectory (y-x projection of Fig. 14). The y-θ projection of Fig. 14 conveys the behavior of the θ component over the course of the three triple-clothoids. θ and x both return to their start values before the dodge maneuver while y has increased during transit down the aisle.

A simpler alternative to the series of triple-clothoid paths in Fig. 14 might be to produce a series of planar-clothoid x-y paths and set the θ orientation as the tangent (tan(y/x)) of the path. However, while this path might appear similar to a triple-clothoid path, a second derivative of θ with respect to distance along the aisle, $d^2\theta/dy^2$, reveals significant differences. If

merely planar-clothoids had been used with the θ orientation set to match the local *x-y* tangent of the planar-clothoid, spikes in the desired θ curvature $d^2\theta/dy^2$ at the beginning and end of each planar-clothoid occur (see the upper portion of Fig. 15). In the lower portion of Fig. 15 it is evident that the triple-clothoid has smoothed out these changes in θ curvature. A user of the Pallet Jack Cobot experiences lower translational accelerations and jerks when the triple-clothoid solution to three-dimensional trajectory generation is used in preference to a modified planar-clothoid solution.

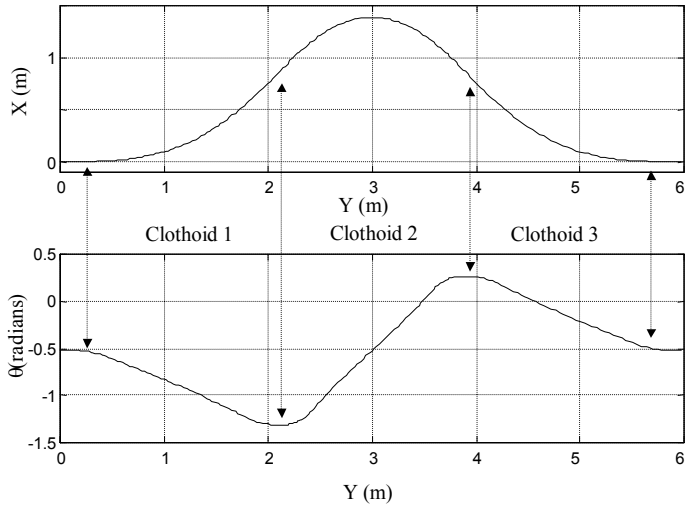

Figure 14. Three triple-clothoids chained together to form a dodge maneuver.

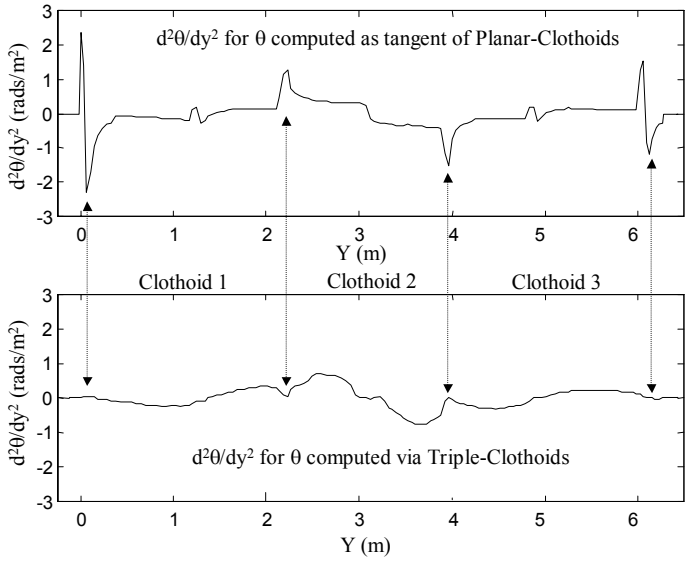

Figure 15. A user of the Pallet Jack Cobot experiences lower linear accelerations and jerks when the triple-clothoid solution to three-dimensional trajectory generation is used in preference to a modified planar-clothoid solution.

CONCLUSIONS

A complete solution to three-dimensional path generation is derived that matches position and tangency requirements at the start and finish of a generated path, as well as curvature continuity along the path. This method combines analytical and numerical steps to give a manageable solution that is coded in a computer algorithm. The triple-clothoid is then implemented for some example tasks and is demonstrated to work effectively.

The triple-clothoid curve is not specified in terms of a single maximum curvature value, as planar-clothoids typically are. However, the resulting curvature has no discontinuities; the original requirement of our three-dimensional curve provided that the initial trajectory has zero curvature. It should also be noted that in the case that the lines are not skew, but are close to intersecting or are coincident, the properly coded equations reduce to a single planar-clothoid.

The triple clothoid solution could be changed slightly to allow *Clothoid 0* to be composed of proximal and distal sections with different rates of linear change in curvature, forming an asymmetrical triple-clothoid. This would change only a single parameter in the equations of *Segments 4* through *8* and allow for more flexible trajectory planning. The description of the out-of-plane curvature of *Clothoids 1* and *2* in Figs. 8 and 9 would become slightly more ambiguous however.

The ratio l_1/a^0 can vary from 0 to 1 but in practice a number between approximately 0.25 and 0.75 is comfortable for operators. No attempt was made to optimize the value of this parameter quantitatively in terms of energy requirements. If the parameter is close to 1, the operator experiences the conversion of the Pallet Jack Cobot's momentum from translational inertia to rotational inertia as an uncomfortable translational acceleration and jerk at the handle-grip in the center region of the triple-clothoid path. This could be avoided by locating the handle pivot point at the center of mass of the Pallet Jack.

The triple-clothoid solution is particularly amenable to *x-y-*θ systems. Since the out-of-plane curvature of the triple-clothoid construction is often the θ component of an *x-y-*θ system (initial and goal trajectories not involving changes in θ), the free parameter l_1/a^0 chooses how much to spread the θ turn over the *x-y Clothoid 0*. Also note that changing the value of l_1/a^0 is equivalent to changing the characteristic length scale factor that relates radians to length (when the out-of-plane curvature is purely the θ component of an *x-y-*θ system).

APPENDIX

Additional properties and formulas for planar-clothoids are defined here. Arc length of the proximal and distal segments of a planar-clothoid $a = a_o p$ where $a_o = \pi\rho p$, ρ is the maximum allowed curvature, and $p = (1-\alpha/\pi)^{1/2}$ (Fig. 2). $\alpha = \pi - \cos^{-1}(T_1^T T_2)$ is the angle between the start and goal tangents. $d =$

$a_o(F_c(p) + F_s(p)\cot(\alpha/2))$ is the distance from the start of the clothoid to the corner. In the case that d is known but maximum curvature ρ is not, $\rho = d/(\pi p(Fc(p) + Fs(p)\cot(\alpha/2)))$. F_c and F_s are functions known as the Fresnel Integrals and a numerical approximation for these unsolvable integrals is found in Heald [3].

Equation 7 defines a proximal coordinate system $\{\boldsymbol{c}_P\}$ located at $\boldsymbol{R}_1$. $\boldsymbol{I}$ is the 3x3 identity matrix.

$$\{\mathrm{c}_P\} = \begin{bmatrix} \mathrm{c}_{P1} \\ \mathrm{c}_{P2} \\ \mathrm{c}_{P3} \end{bmatrix} = \begin{bmatrix} \mathrm{T}_1 \\ \frac{(\mathrm{I}-\mathrm{T}_1\mathrm{T}_1{}^T)(\mathrm{T}_2-\mathrm{T}_1)}{\left|(\mathrm{I}-\mathrm{T}_1\mathrm{T}_1{}^T)(\mathrm{T}_2-\mathrm{T}_1)\right|} \\ \mathrm{c}_{P1}\times\mathrm{c}_{P2} \end{bmatrix} \tag{7}$$

Equation 8 defines a distal coordinate system $\{\boldsymbol{c}_D\}$ located at $\boldsymbol{R}_3$.

$$\{\mathrm{c}_D\} = \begin{bmatrix} \mathrm{c}_{D1} \\ \mathrm{c}_{D2} \\ \mathrm{c}_{D3} \end{bmatrix} = \begin{bmatrix} \mathrm{T}_2 \\ \frac{(\mathrm{I}-\mathrm{T}_2\mathrm{T}_2{}^T)(\mathrm{T}_2-\mathrm{T}_1)}{\left|(\mathrm{I}-\mathrm{T}_2\mathrm{T}_2{}^T)(\mathrm{T}_2-\mathrm{T}_1)\right|} \\ \mathrm{c}_{D1}\times\mathrm{c}_{D2} \end{bmatrix} \tag{8}$$

Formulas to evaluate the planar-clothoid's position vector $\boldsymbol{R}(s)$, unit tangent vector $\boldsymbol{T}(s)$, unit normal vector $\boldsymbol{N}(s)$ and curvature magnitude $\kappa(s)$ are given below. Three sets of equations are required; one for the proximal clothoid segment ($0 \le s < a$), one for distal clothoid segment ($a \le s < 2a$) and one for the final tangent $\boldsymbol{T}_2$ ($2a \le s$).

$$\mathrm{R}(s) = \begin{cases} \mathrm{R}_2 + (a_o F_c(\frac{s}{a_o}) - d)\mathrm{c}_{P1} + a_o F_s(\frac{s}{a_o})\mathrm{c}_{P2} & 0 \le s < a \\ \mathrm{R}_2 + (d - a_o F_c(2p - \frac{s}{a_0}))\mathrm{c}_{D1} + a_o F_s(2p - \frac{s}{a_o})\mathrm{c}_{D2} & a \le s < 2a \\ \mathrm{R}_2 + (s + d - 2p)\mathrm{T}_2 & 2a \le s \end{cases} \tag{9}$$

$$\boldsymbol{T}(s) = \begin{cases} \cos(\frac{s^2}{2\rho a})\boldsymbol{c}_{P1} + \sin(\frac{s^2}{2\rho a})\boldsymbol{c}_{P2} & 0 \le s < a \\ \cos(\frac{(2a-s)^2}{2\rho a})\boldsymbol{c}_{D1} - \sin(\frac{(2a-s)^2}{2\rho a})\boldsymbol{c}_{D2} & a \le s < 2a \\ \boldsymbol{T}_2 & 2a \le s \end{cases} \tag{10}$$

$$\boldsymbol{N}(s) = \begin{cases} -\sin(\frac{s^2}{2\rho a})\boldsymbol{c}_{P1} + \cos(\frac{s^2}{2\rho a})\boldsymbol{c}_{P2} & 0 \le s < a \\ \sin(\frac{(2a-s)^2}{2\rho a})\boldsymbol{c}_{D1} + \cos(\frac{(2a-s)^2}{2\rho a})\boldsymbol{c}_{D2} & a \le s < 2a \\ \boldsymbol{c}_{D2} & 2a \le s \end{cases} \tag{11}$$

$$\kappa(s) = \begin{cases} \frac{s}{\rho a} & 0 \le s < a \\ \frac{2a-s}{\rho a} & a \le s < 2a \\ 0 & 2a \le s \end{cases} \tag{12}$$

AKNOWLEDGEMENTS

We would like to thank Witaya Wannasuphoprasit for building the original "Scooter" cobot.

This material is based upon work supported by the National Science Foundation under Grant No. 9988437.

WORKS CITED

1. Michael Peshkin, J. Edward Colgate, Witaya Wannasuphoprasit, Carl Moore, Brent Gillespie, 2001, "Cobot Architecture**,"** IEEE Transactions on Robotics and Automation, **17**(4), pp 377.

2. Schmitt, P. R. and W. J. Book, 1996, "Reactive Path Shaping: Local Path Planning for Autonomous Mobile Robots," Proceedings of the ASME Dynamic Systems and Controls Division, **58**, pp. 639-646.

3. Heald, M. A., 1985, "Rational Approximations for the Fresnel Integrals," Mathematics of Computation, **44(**170), pp. 459-461.

4. Barnhill, R. E. and R. F Riesenfeld, 1974, Computer Aided Geometric Design, Academic Press, New York, pp. 173-205.

5. Faux, I. D. and M. J. Pratt, 1979, Computational Geometry for Design and Manufacture, John Wiley and Sons, New York, pp. 99-104.